IEEE Access
Multidisciplinary ⋮ Rapid Review ⋮ Open Access Journal

Received February 2, 2021, accepted February 8, 2021, date of publication February 16, 2021, date of current version March 4, 2021.

Digital Object Identifier 10.1109/ACCESS.2021.3059889

A Robust Hybrid Position/Force Control Considering Motor Torque Saturation

TAKASHI OHHIRA[1], KEINOSUKE YOKOTA[1], SHUICHI TATSUMI[1], AND TOSHIYUKI MURAKAMI[2], (Senior Member, IEEE)

[1]Graduate School of Science and Technology, Keio University, Yokohama 223-8522, Japan
[2]Department of System Design Engineering, Keio University, Yokohama 223-8522, Japan

Corresponding author: Takashi Ohhira (ohhira@sum.sd.keio.ac.jp)

This work was supported in part by KEIRIN JKA under Grant 2020M-127.

ABSTRACT This paper proposes a robust hybrid position/force control (HPFC) system for multi-degree of freedom manipulators (MDoFMs) with torque constraints on each joint. General HPFC systems can control the interactive contact forces and positions of manipulators in various environments. In HPFC systems, to improve the control performance for MDoFMs, motor torque saturation should be considered. Thus, a robust HPFC system that considers torque constraints by predictive functional control (PFC) is proposed in this paper. The proposed method simultaneously handles the response characteristics and torque constraints of actuators by using PFC as joint space position controllers. Additionally, the robustness of actuators against external forces is enhanced, and the model parameter errors are compensated by the disturbance observer technique. Moreover, implicit force control law and inverse kinematics are introduced for the workspace position/force control to implement the joint space position controllers. Consequently, the stability and robustness of the actuators are considered, and suitable position/force control can be performed even if the torque is saturated. The validity of the proposed method is tested with three planar manipulator joints with a uniaxial force sensor.

INDEX TERMS Force control, manipulators, optimal control, position control, predictive control.

I. INTRODUCTION

Hybrid position/force control (HPFC) [1], [2] is a control method for the positions and forces of multi-degree of freedom manipulators (MDoFM), by which it is possible to control the position/attitude and the force/moment on the workspace states of manipulators. HPFC has been applied to bilateral control [3], [4], continuum robots [5], polishing [6], microhandling [7], quadruped robots [8], rehabilitation robots [9], assembly robots [10], and cooperative polishing tasks [11]. Unfortunately, guaranteed motion generation against external forces by HPFC is a serious challenge for the practical application of manipulator systems, such as human-robot collaboration. In general hybrid control systems, the control variables on the workspace are decomposed into the dimensions of position and force, and the control inputs are derived by integrating both control inputs through a Jacobian matrix (differential kinematics). This method does not consider the motion and torque of the joint space. Thus, problems related to the saturation of input torque, such as excessive overshoot and vibration, remain. Moreover, the torque saturation caused by external forces from contact with unknown objects can result in unstable robot behavior. To prevent unstable motion, an HPFC method that considers constraints imposed on each actuator should be developed.

Alternatively, impedance control [12]–[14] and variable impedance control [15]–[17] have both been proposed as control methods for position and force. The impedance control law (ICL) is a control method for position and force in the workspace. Thus, the ICL cannot directly handle the constraints imposed on each actuator, and, accordingly, the method can cause several problems, such as unstable behavior, hunting motion, bouncing motion, and the application of excessive force to the skin. Kikuuwe [13] developed torque-bounded admittance control and demonstrated that position-based force control considering torque saturation is useful in realizing safe behavior for a single-axis force controller. By contrast, to achieve HPFC via a joint space

The associate editor coordinating the review of this manuscript and approving it for publication was Wonhee Kim.

controller, implicit force control methods [18]–[21] have been proposed, which indirectly control the force by position or velocity control in the joint space. For implicit control methods, an inner-loop controller determines the response characteristics of the actuator, and, thus, it is assumed that this method avoids unstable behavior associated with impedance control and HPFC due to considering input torque saturation. Ohishi *et. al.* [22] demonstrated that a control system that considers torque saturation can contribute to the execution of high-speed motion control. Additionally, this control system considering torque saturation is useful with respect to avoiding machine failure due to unexpected external force.

This paper proposes a robust HPFC strategy for MDoFMs that considers the torque saturation of each joint. The proposed position/force control uses the position control in the joint space to consider torque saturation and to avoid the unstable state of force control when an unknown object comes into contact. To consider the torque saturation, a joint space position controller is used and its reference is derived by utilizing inverse kinematics [23] based on the workspace position reference modified by the implicit control law. Additionally, the proposed method uses predictive functional control (PFC) [24]–[27], which is a model predictive control (MPC) strategy, as the joint space position controller. MPC is well-known as a method that can systematically handle the control input and output constraints of robots. The main drawbacks are high computational load and accurate internal model design. For instance, if MPC is applied to a force control manipulator in an unknown environment, the force control cannot be implemented because environmental parameters are not available in the internal model. By contrast, the force control part of the proposed method is implicitly achieved by the position control of the joint space, which means that MPC is only applicable for plant parameters. However, achieving precise force control requires a high control frequency, which may not be possible with normal linear MPC. PFC can implement by high control frequency due to avoiding online optimization while securing the control input constraint. Therefore, it is an effective method for considering torque saturation. However, it is challenging to apply PFC to MDoFM systems, because it mainly targets single-input/single-output (SISO) systems. To apply PFC to an MDoFM, it is necessary to use the disturbance observer (DOB) method [28]–[35], which is a control technique that estimates modeling errors and external forces as input disturbances and cancels them to nominalize the plant model. Applying DOB to MDoFM is possible to independently control each joint as a SISO system because of construct acceleration control with decoupling using the nominal inertia matrix. Thus, the proposed method uses the DOB-based acceleration control system of the joint space by applying PFC to MDoFM systems. Moreover, the decoupling-based control system of the manipulator can determine the control response of each joint independently, so it is easy to use and consider redundancy. Additionally, the proposed method can perform disturbance cancellation and high-speed motion control in consideration of torque saturation, which is also useful for profitability improvement. An experiment involving a planar three-link manipulator control is conducted to demonstrate the validity and usefulness of the proposed method.

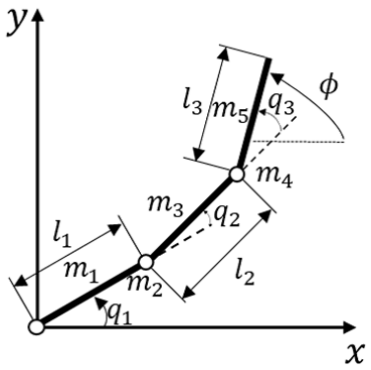

FIGURE 1. Model of the three-link manipulator.

This paper is organized as follows; Section II provides mathematical modeling; Section III proposes a novel position/force control and provides each component; Section IV shows the experimental results on position/force control, guaranteed motion against external forces, and additional experimental results on the utilization of redundancy; and Section V concludes by providing application examples of the proposed method.

II. PRELIMINARIES

A. MATHEMATICAL MODELING

This paper uses the planar three-link manipulator to verify the proposed method. Fig. 1 shows the model of this manipulator. It can determine the position and attitude of the end-effector on a plane. Additionally, if the attitude can be controlled appropriately, accurate force control is possible with a single-axis force sensor. Thus, it is suitable for the experimental verification of HPFC systems. First, the joint angle vector ($\boldsymbol{q}$) and the input torque vector ($\boldsymbol{\tau}$) are defined as $\boldsymbol{q} = [q_1 \;\; q_2 \;\; q_3]^T$ and $\boldsymbol{\tau} = [\tau_1 \;\; \tau_2 \;\; \tau_3]^T$, respectively. Then, the position vector and end-effector attitude in the workspace can be defined as $\boldsymbol{X} = [x \;\; y \;\; \phi]^T$. In the joint space, using the Lagrange equation, the equations of motion are given by

$$\ddot{\boldsymbol{q}} = \frac{1}{\boldsymbol{J}}\{\boldsymbol{\tau} - \boldsymbol{D}(\dot{\boldsymbol{q}}) - \boldsymbol{H}(\boldsymbol{q}, \dot{\boldsymbol{q}}) - \boldsymbol{\tau}_{\mathrm{dis}}\}, \tag{1}$$

where $\boldsymbol{J}$, $\boldsymbol{D}$, and $\boldsymbol{H}$ denote the inertial matrix, friction function, and centrifugal force and Coriolis force functions, respectively. $\boldsymbol{\tau}_{\mathrm{dis}}$ denotes the disturbance torque generated by external force and modeling errors. The workspace position utilizing forward kinematics is given by

$$\boldsymbol{X} = \begin{bmatrix} J_{a1} & J_{a2} & J_{a3} \end{bmatrix}^T, \tag{2}$$

where $J_{a1} = L_1 \cos q_1 + L_2 \cos(q_1 + q_2) + L_3 \cos(q_1 + q_2 + q_3)$, $J_{a2} = L_1 \sin q_1 + L_2 \sin(q_1 + q_2) + L_3 \sin(q_1 + q_2 + q_3)$, and $J_{a3} = q_1 + q_2 + q_3$.

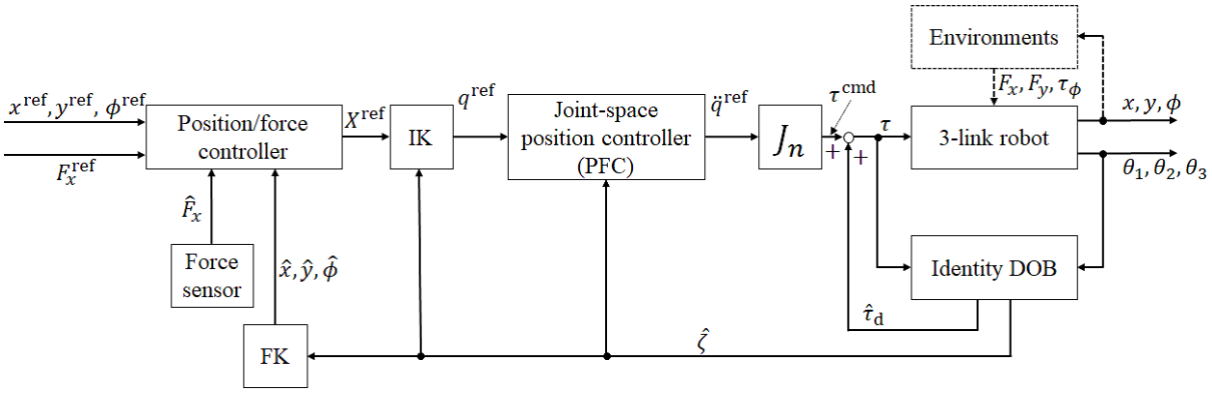

FIGURE 2. System diagram of the proposed method. IK and FK denote inverse kinematics and forward kinematics, respectively.

Moreover, the differential kinematics that translate the velocities in the workspace and joint space can be described as

$$\dot{\boldsymbol{X}} = \boldsymbol{J}_{aco}\dot{\boldsymbol{q}} \tag{3}$$

where $\boldsymbol{J}_{aco}$ denotes a 3×3 Jacobian matrix, which can be obtained by partial differentiation of (2). The Jacobian matrix is related to $\boldsymbol{q}$, which is represented by $\boldsymbol{J}_{aco}(\boldsymbol{q})$; however, $(\boldsymbol{q})$ is omitted in this paper.

III. PROPOSED CONTROL SYSTEM

Fig. 2 shows the system diagram. The proposed method comprises four components: 1) DOB to improve robustness and nominalize the plant model as well as to design the acceleration control, 2) implicit force control law in the workspace to transform the force reference to the position reference, 3) inverse kinematics to convert the modified workspace position reference to the joint space position reference, and 4) PFC for the joint space acceleration control system considering torque saturation. This section describes the case of force control on the x-axis.

A. IDENTITY DISTURBANCE OBSERVER AND ACCELERATION CONTROL

DOB can be used to estimate and cancel modeling errors, parameter errors, and external disturbances. If the disturbances can be estimated accurately, the stability and tracking performance of the control system can be improved. Additionally, DOB-based control systems ensure robust motion control as well as overall plant robustness by feedbacking the disturbance estimates [32]. Fig. 3 shows the basic structure of the DOB, where $\boldsymbol{J}_n$, g_w, and $\ddot{\boldsymbol{q}}^{\mathrm{ref}}$ denote the nominal inertia matrix, the cutoff frequency of the lowpass filter used in the DOB, and the acceleration reference, respectively. This DOB estimates and cancels the disturbance torque $(\boldsymbol{\tau}_d)$ which is the torque generated from other than the nominalized model with the inertial matrix. Additionally, acceleration control can be transparently conducted by multiplying the input from the upper controller by the nominal inertia matrix. Consequently,

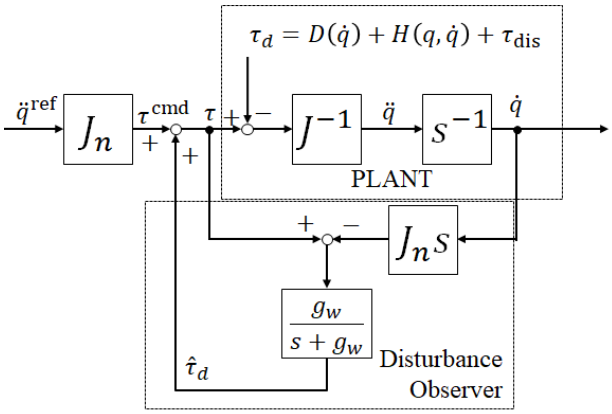

FIGURE 3. Basic concepts of acceleration control by DOB.

the internal model of the upper controller is nominalized by the DOB.

Generally, the DOB is obtained using a minimal-order state observer to estimate the disturbance. However, PFC, which is a model-based control method, requires state vector information, including velocity in the joint space. Thus, this study utilizes the identity DOB (IDOB) [35] on the basis of state-space observers. The IDOB not only estimates the disturbance but also simultaneously estimates the velocity of the joint space and the actual value of the measured variables contaminated by noise, by which the influence of noise on the feedback loop can be reduced. Moreover, the simultaneous estimation of state and disturbance should improve the estimation accuracy. Fig. 4 shows the IDOB design method in the joint space. First, the equation of estimated disturbance is given by

$$\hat{\boldsymbol{\tau}}_{\mathrm{d}} = \boldsymbol{D}(\dot{\boldsymbol{q}}) + \boldsymbol{H}(\boldsymbol{q}, \dot{\boldsymbol{q}}) + \boldsymbol{\tau}_{\mathrm{dis}}. \tag{4}$$

This disturbance equation is utilized to implement acceleration control and nominalize the plant model with the nominal inertia matrix.

Then, a state vector including position and velocity as $\boldsymbol{\zeta} = [\boldsymbol{q}^T \ \ \dot{\boldsymbol{q}}^T]^T$ is defined. Additionally, to simultaneously

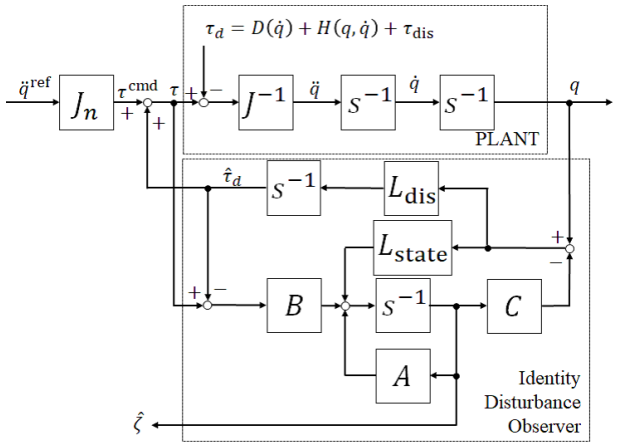

FIGURE 4. Acceleration control by IDOB.

estimate the state and the disturbance, the extended state vector including disturbance is defined by $\bar{\boldsymbol{\zeta}} = [\boldsymbol{\zeta}^T \quad \boldsymbol{\tau}_d^T]^T$. The extended state space model is given by

$$\begin{aligned}\begin{bmatrix}\dot{\hat{\boldsymbol{\zeta}}}\\ \dot{\hat{\boldsymbol{\tau}}}_d\end{bmatrix} &= \bar{\boldsymbol{A}}\hat{\bar{\boldsymbol{\zeta}}} + \bar{\boldsymbol{B}}\boldsymbol{\tau},\\ &= \begin{bmatrix}\boldsymbol{A} & -\boldsymbol{B}\\ \boldsymbol{0} & \boldsymbol{0}\end{bmatrix}\begin{bmatrix}\hat{\boldsymbol{\zeta}}\\ \hat{\boldsymbol{\tau}}_d\end{bmatrix} + \begin{bmatrix}\boldsymbol{B}\\ \boldsymbol{0}\end{bmatrix}\boldsymbol{\tau}, \qquad (5)\\ \boldsymbol{y} = \bar{\boldsymbol{C}}\hat{\bar{\boldsymbol{\zeta}}} &= \begin{bmatrix}\boldsymbol{C} & \boldsymbol{0}\end{bmatrix}\begin{bmatrix}\hat{\boldsymbol{\zeta}}\\ \hat{\boldsymbol{\tau}}_d\end{bmatrix}, \qquad (6)\end{aligned}$$

where $\boldsymbol{A}$, $\boldsymbol{B}$, $\boldsymbol{C}$, and $\boldsymbol{0}$ denote the system matrix, the input matrix, the output matrix, and a zero matrix with appropriate orders, respectively. Accordingly, $\bar{\boldsymbol{A}}$, $\bar{\boldsymbol{B}}$, and $\bar{\boldsymbol{C}}$ are the system, input, and output matrices for the extended system, respectively.

These matrices, which are based on the disturbance estimation of (4), can be described as

$$\boldsymbol{A} = \begin{bmatrix}\boldsymbol{0} & \boldsymbol{I}\\ \boldsymbol{0} & \boldsymbol{0}\end{bmatrix}, \qquad (7)$$

$$\boldsymbol{B} = \begin{bmatrix}\boldsymbol{0}\\ \boldsymbol{J}_n^{-1}\end{bmatrix}, \qquad (8)$$

$$\boldsymbol{C} = \begin{bmatrix}\boldsymbol{I} & \boldsymbol{0}\end{bmatrix}, \qquad (9)$$

where $\boldsymbol{I}$ is a 3×3 identity matrix and $\boldsymbol{0}$ denotes a 3×3 dimension zero matrix.

The equation of this IDOB system is given by

$$\begin{aligned}\dot{\bar{\boldsymbol{\zeta}}} &= (\bar{\boldsymbol{A}} - \boldsymbol{L}\bar{\boldsymbol{C}})\bar{\boldsymbol{\zeta}} + \bar{\boldsymbol{B}}\boldsymbol{\tau} + \boldsymbol{L}\boldsymbol{y}, \qquad (10)\\ &= (\bar{\boldsymbol{A}} - \begin{bmatrix}\boldsymbol{L}_{\text{state}}\\ \boldsymbol{L}_{\text{dis}}\end{bmatrix}\bar{\boldsymbol{C}})\bar{\boldsymbol{\zeta}} + \bar{\boldsymbol{B}}\boldsymbol{\tau} + \begin{bmatrix}\boldsymbol{L}_{\text{state}}\\ \boldsymbol{L}_{\text{dis}}\end{bmatrix}\boldsymbol{y}, \qquad (11)\end{aligned}$$

where $\boldsymbol{L}$ is the observer gain of the IDOB and is configured by observer gains for state ($\boldsymbol{L}_{\text{state}}$) and disturbance ($\boldsymbol{L}_{\text{dis}}$). To compensate for the stability of the IDOB, the observer gain should be designed so that all eigenvalues of $(\bar{\boldsymbol{A}} - \boldsymbol{L}\bar{\boldsymbol{C}})$ are negative. This can be achieved by utilizing the pole placement method or the linear quadratic regulator method. In this paper, the pole placement method was utilized to design the IDOB. By using IDOB, it is possible to obtain estimates that are less sensitive to noise compared with conventional DOB.

B. REFERENCE GENERATOR FOR IMPLICIT FORCE CONTROL

In this section, the method of converting a workspace force reference ($\boldsymbol{F}^{\text{ref}}$) into a modified workspace position reference ($\boldsymbol{X}^{\text{ref}}$) is explained. In the experimental verification, force control was performed on the x-axis, and position/attitude control was performed for other variables (y, ϕ). Thus, the explanation in this section concerns converting F_x^{ref} to x^{ref}.

The conversion of the nominal position reference (x_n^{ref}) in position-based impedance control is given by,

$$x_n^{\text{ref}} = x_{\text{cp}} + \frac{1}{K_e}F_x^{\text{ref}}, \qquad (12)$$

where x_{cp} and K_e denote the known contact position and environmental stiffness, respectively. Applying the force control based on the known environmental parameters of (12) is challenging because of the difficulty involved in handling uncertain environments. Moreover, applying excessive force is possible because of variation in contact point and stiffness. Additionally, such a single control system cannot handle various objects.

To achieve force control in various unknown environments through position control, this paper proposes a modified nominal impedance reference, which is given by

$$x^{\text{ref}} = x + \frac{1}{K_f}(F_x^{\text{ref}} - F_x), \qquad (13)$$

$$\tilde{x} = \frac{1}{K_f}(F_x^{\text{ref}} - F_x), \qquad (14)$$

$$x^{\text{ref}} = x + \tilde{x}, \qquad (15)$$

where $1/K_f$ is the gain required to convert the force error to the position reference and F_x denotes a measured force of the x-axis in the workspace. The force feedback is integrated into the position reference, as shown by (13). Equation (15) makes it possible to consider the contact velocity of the environment and the force reference. Generally, control parameter designs of the force control system for unknown environments are smaller than those of the position control system. By contrast, the proposed reference generation method achieves high-speed force control based on position control. Therefore, the proposed method converges with the force reference faster than direct force control systems. This helps to suppress impact force, hunting motion, and bouncing motion during a collision. When performing position control for all directions, the proposed method directly inputs the position reference value to all state variables.

C. INVERSE KINEMATICS

In this paper, the implicit workspace force control by the joint space position control is utilized to consider the stability of contact motion and torque saturation. The implementation of the proposed method requires the conversion of the position

reference ($\boldsymbol{X}^{\mathrm{ref}}$) in the workspace to the position reference ($\boldsymbol{q}^{\mathrm{ref}}$) in the joint space. In this paper, the inverse kinematics based on the Levenvetg-Marquardt method [23] applied in several previous studies are utilized with small modifications made to avoid singular points in the workspace state of the robot. The inverse kinematics equations are given by

$$\boldsymbol{q}^{\mathrm{ref}}(k) = \boldsymbol{q}(k) + \tilde{\boldsymbol{q}}^{\mathrm{ref}}(k), \tag{16}$$

$$\tilde{\boldsymbol{q}}^{\mathrm{ref}}(k) = \boldsymbol{H}(k)\,\boldsymbol{M}(k), \tag{17}$$

$$\boldsymbol{H}(k) = \{\boldsymbol{J}_{aco}^{T}(k)\,\boldsymbol{W}_e\boldsymbol{J}_{aco}(k) + \boldsymbol{W}_n(k)\}^{-1}, \tag{18}$$

$$\boldsymbol{M}(k) = \boldsymbol{J}_{aco}^{T}(k)\,\boldsymbol{W}_e\boldsymbol{X}_e(k) + \boldsymbol{X}_e(k), \tag{19}$$

$$\boldsymbol{W}_e = \mathrm{diag}(w_1, w_2, w_3), \tag{20}$$

$$\boldsymbol{W}_n(k) = \mathrm{diag}(\boldsymbol{X}_e(k)) + \lambda\boldsymbol{I}, \tag{21}$$

where k denotes the current sample time. This study avoids singularities in the workspace by applying a small bias $\lambda(=10^{-8})$ and the workspace error vector to (21). $\boldsymbol{W}_e$ is a diagonal matrix with weights (w_1, w_2, and w_3) for each joint angle. $\boldsymbol{W}_n$ is a damping factor and a diagonal matrix of error vectors in the workspace. $\boldsymbol{X}_e$ is a position error vector in the workspace. By using this method, it is possible to maintain control from the singular point of the manipulator, and it is also possible to calculate the inverse kinematics considering the precise initial positioning and the variation reference ($\tilde{\boldsymbol{q}}^{\mathrm{ref}}$). In this paper, speed constraints are imposed for $\tilde{\boldsymbol{q}}^{\mathrm{ref}}$ by a nominal speed (30 rad/s) of an actual motor which can be defined as $2\pi\cdot 30/60 = \pi$[rad/s]. Indeed, control based on the joint angle is useful, because it can utilize initial workspace position/attitude-based angles calculated offline to avoid singular points, which are essential for precise initial positioning.

D. JOINT SPACE POSITION CONTROLLER

The joint space controller comprises PFC and an acceleration controller based on the IDOB. PFC is one of many MPC strategies. Generally, several MPC systems aim to control multi-input/multi-output systems explicitly by considering input and output constraints through real-time optimization. By contrast, PFC systems aim to control SISO systems explicitly by considering control input constraints. Although PFC cannot consider output constraints, it can be implemented with a higher control frequency than general MPC systems, because real-time optimization is not necessary. Thus, it is easy to replace the proportional-derivative (PD) control utilized in general DOB-based acceleration control systems with PFC systems. Furthermore, the two main control parameters of PFC include the target settling time and the damping factor for tracking errors when making predictions. Accordingly, it is easier to design a controller considering the torque saturation and the response of each link with a PFC system than it is with a PD system.

In the proposed method, an independent PFC system for each joint is utilized as the position control system. In designing the PFC systems, each joint is decoupled by the IDOB. Consequently, each joint is decoupled on the joint controller, and, accordingly, it is possible to output the acceleration reference of each joint and perform joint position control while considering each joint torque independently. Additionally, a control parameter of the PFC system is expressed as the target settling time, so that the response of each joint can be set explicitly and independently. Consequently, by utilizing PFC and considering actuator saturation, the proposed method can be designed such that the response time is constant for different output actuators.

The main problem with utilizing model-based control systems is associated with the derivation of internal models. In model-based systems, the parameter errors of internal models can reduce the tracking control performance. However, the internal model for the proposed PFC is markedly unlike internal models utilized in several conventional model-based control system designs; particularly, it utilizes $1/s^2$ by utilizing the nominalization and the acceleration control. Thus, the design of the internal model of the PFC does not require physical parameters, and it is easy to adjust the control performance. It should be pointed out that this advantage is obtained from the DOB-based acceleration control. Unfortunately, the offset-free characteristics of the PFC are dependent on disturbance estimation and rejection by the IDOB. The PFC design method follows [27]; only the internal model and the constraints for designing the proposed method are explained, focusing on the first joint angle (q_1).

1) INTERNAL MODEL

An independent joint space state vector $\boldsymbol{x}_q = [q_1 \;\; \dot{q}_1]$ is defined based on the state estimates of the IDOB, and, as an internal model of the PFC, the discrete-time state space model can be described as

$$\boldsymbol{x}_q(k+1) = \boldsymbol{A}_q\boldsymbol{x}_q(k) + \boldsymbol{B}_q u(k), \tag{22}$$

$$y(k) = \boldsymbol{C}_q\boldsymbol{x}_q(k), \tag{23}$$

where each coefficient matrix is defined as

$$\boldsymbol{A}_q = \begin{bmatrix} 1 & T_s \\ 0 & 1 \end{bmatrix}, \tag{24}$$

$$\boldsymbol{B}_q = \begin{bmatrix} 0 \\ T_s \end{bmatrix}, \tag{25}$$

$$\boldsymbol{C}_q = \begin{bmatrix} 1 & 0 \end{bmatrix}. \tag{26}$$

where T_s is the sampling period of time. Note that the control input (u) denotes the acceleration reference ($\ddot{q}_1^{\mathrm{ref}}$) and the internal model does not utilize the physical parameters.

2) OUTLINE OF CONTROL SCHEME

The derivation of the acceleration reference is described in this section. The derivation method as a control input is based on [26] and [27]. An element of reference trajectory ($T(k+i)$) in a prediction horizon is given by

$$T(k+i) = s(k+i) - \alpha^i(s(k) - y(k)), \tag{27}$$

where s represents the set point value, which is the joint angle reference obtained by inverse kinematics, and α is a

damping factor for the trajectory reference, which, following [27], is described as

$$\alpha = e^{-3T_s/T_{\rm ref}}, \tag{28}$$

where $T_{\rm ref}$ is the target response time of the closed-loop, which is a control parameter determining the plant response. In this paper, α is fixed by (28), and, thus, $T_{\rm ref}$ is the main controller parameter. Additionally, PFC does not require the optimization of all sample points in a predictive horizon. To calculate the optimal control input, coincidence points, which denote the calculation points, are defined on the reference trajectory. In this study, the coincidence points (h_j) can be defined as

$$h_j = T_{\rm ref}/(T_s(n-j+1)), \tag{29}$$

where $h_j (j = 1, 2, \ldots, n)$ represents the sample time of coincidence points and n is the number of coincidence points (n is also one of the controller parameters).

The cost function (V) utilizing the coincidence points based on error correction between the output prediction ($\hat{y}$) and the reference trajectory is given by

$$V(k) = \sum_{j=1}^{n}\{\hat{y}(k+h_j) - T(k+h_j)\}^2, \tag{30}$$

$$= \sum_{j=1}^{n}\{y_b(h_j)^T\mu(k) + C_q(A_q^{h_j} - I)\boldsymbol{x}_q(k) + (\alpha^{h_j} - 1)(s(k) - y(k))\}^2. \tag{31}$$

where μ $(1, 2, \ldots, n)$ is the decision variable for determining the control input. The control input for prediction and optimization at each coincident point is designed by a prespecified combination of base functions, such as step, ramp, and parabola [25], [26]. $y_b(h_j)$ is the plant response to each base function input. For example, the system response to the first coincidence point ($n = 3$) is given by

$$y_b(h_j) = \boldsymbol{\Theta}(h_j)\boldsymbol{u}_{\rm s} + \boldsymbol{\Theta}(h_j)\boldsymbol{u}_{\rm r} + \boldsymbol{\Theta}(h_j)\boldsymbol{u}_{\rm p} \tag{32}$$

where $\boldsymbol{\Theta} = [\boldsymbol{C}_q\boldsymbol{A}_q^{h_j}\boldsymbol{B}_q \ \ldots \ \boldsymbol{C}_q\boldsymbol{A}_q^{0}\boldsymbol{B}_q \in \mathbb{R}^{h_j}]$, $\boldsymbol{u}_{\rm s} = [1 \ \ldots \ 1]^T \in \mathbb{R}^{h_j}$, $\boldsymbol{u}_{\rm r} = [0 \ T_s \ 2T_s \ \ldots \ h_jT_s]^T \in \mathbb{R}^{h_j}$, and $\boldsymbol{u}_{\rm p} = [0 \ (T_s)^2 \ (2T_s)^2 \ \ldots \ (h_jT_s)^2]^T \in \mathbb{R}^{h_j}$. PFC predicts the future state by utilizing the forced response by the base function and the free response of the system ($\boldsymbol{C}_q\boldsymbol{A}_q^i\boldsymbol{x}_q(k)$). The actual optimal control input is μ, and its closed-form solution is given by

$$\boldsymbol{\mu}(k) = -\{\sum_{j=1}^{n}\{y_b(h_j)y_b(h_j)^T\}^{-1} \times \sum_{j=1}^{n}\{\boldsymbol{C}_q(\boldsymbol{A}_q^{h_j}) - \boldsymbol{I})\boldsymbol{x}_q(k) + (\alpha^{h_j} - 1)(s(k) - y(k))\}y_b(h_j). \tag{33}$$

The first element of μ is the optimal control input based on the receding horizon control.

3) TORQUE CONSTRAINTS

PFC systems can consider control input constraints. However, the PFC in the proposed method derives the acceleration reference for each joint angle. Therefore, the PFC can directly treat constraints on the acceleration reference. In this paper, the torque constraint, which is the actual and essential control input for stable manipulator control, is imposed by the PFC. Furthermore, the constraints are useful for avoiding wind-up problems [36], [37] with respect to DOB estimation. The torque constraint utilizing the limit value ($\tau_{\rm limit}$) determined from the maximum current and torque constant is given by

$$-\tau_{limit} \le \tau_1 \le \tau_{\rm limit}. \tag{34}$$

The actual torque input utilizing the acceleration reference and disturbance estimate at the current time (k) is given by

$$\tau_1(k) = j_n\ddot{q}_1^{\rm ref}(k) + \hat{\tau}_d(k), \tag{35}$$

where j_n denotes the nominal inertia for q_1. The torque constraint is deformed by utilizing the PFC output, which is described by

$$-\tau_{\rm limit} \le j_n\ddot{q}_1^{\rm ref}(k) + \hat{\tau}_d(k) \le \tau_{\rm limit}, \tag{36}$$

$$j_n^{-1}(-\tau_{\rm limit} - \hat{\tau}_d(k)) \le \ddot{q}_1^{\rm ref}(k) \le j_n^{-1}(\tau_{\rm limit} - \hat{\tau}_d(k)). \tag{37}$$

The PFC system utilizing this constraint can derive the acceleration reference that explicitly considers the torque constraint.

4) STABILITY ANALYSIS

The stability of the proposed system is demonstrated by the number of coincidence points ($n = 3$) utilized in the experiments. The actual PFC system, which is represented by (33), is a linear time-invariant controller with a closed-form optimal solution. The actual control input ($\mu_1 = \ddot{q}_1^{\rm ref}$) with ($n = 3$) is given by

$$\mu_1 = \boldsymbol{f}_{fo}\{\boldsymbol{r}_{fi}(q_1^{\rm ref} - \hat{q}_1) - \boldsymbol{f}_{fr}\hat{\boldsymbol{x}}_q + \boldsymbol{I}^{3\times1}\hat{q}_1\}, \tag{38}$$

where $\boldsymbol{f}_{fo} \in \mathbb{R}^n$, $\boldsymbol{r}_{fi} = [1-\alpha^{h_1} \ 1-\alpha^{h_2} \ 1-\alpha^{h_3}]^T \in \mathbb{R}^n$, and $\boldsymbol{f}_{fr} = [\boldsymbol{C}_q\boldsymbol{A}_q^{h_1} \ \boldsymbol{C}_q\boldsymbol{A}_q^{h_2} \ \boldsymbol{C}_q\boldsymbol{A}_q^{h_3}]^T \in \mathbb{R}^{n\times2}$ denote the vector regarding μ_1 of the inverse matrix of forced response (y_b), the reference filtering vector, and the free-response vector, respectively. By utilizing (23), the position elements of $\boldsymbol{f}_{fr}$ are $\boldsymbol{f}_{fr,1,1}, \boldsymbol{f}_{fr,2,1}, \boldsymbol{f}_{fr,3,1} = 1$, where $\boldsymbol{f}_{fr,v,w}$ denotes the elements of v-th row and w-th column in $\boldsymbol{f}_{fr}$. Thus, the control input obtained by decomposing each matrix element is given by

$$\begin{aligned}\mu_1 &= \boldsymbol{f}_{fo,1}\{\boldsymbol{r}_{fi,1}(q_1^{\rm ref} - \hat{q}_1) - \boldsymbol{f}_{fr,1,2}\hat{\dot{q}}_1\} \\ &\quad + \boldsymbol{f}_{fo,2}\{\boldsymbol{r}_{fi,2}(q_1^{\rm ref} - \hat{q}_1) - \boldsymbol{f}_{fr,2,2}\hat{\dot{q}}_1\} \\ &\quad + \boldsymbol{f}_{fo,3}\{\boldsymbol{r}_{fi,3}(q_1^{\rm ref} - \hat{q}_1) - \boldsymbol{f}_{fr,3,2}\hat{\dot{q}}_1\}, \\ &= k_p(q_1^{\rm ref} - \hat{q}_1) - k_d\hat{\dot{q}}_1,\end{aligned} \tag{39}$$

where $k_p = (\boldsymbol{f}_{fo,1}\boldsymbol{r}_{fi,1} + \boldsymbol{f}_{fo,2}\boldsymbol{r}_{fi,2} + \boldsymbol{f}_{fo,3}\boldsymbol{r}_{fi,3})$ and $k_d = (\boldsymbol{f}_{fo,1}\boldsymbol{f}_{fr,1,2} + \boldsymbol{f}_{fo,2}\boldsymbol{f}_{fr,2,2} + \boldsymbol{f}_{fo,3}\boldsymbol{f}_{fr,3,2})$. From (40), the PFC

system without the constraints used in this paper can approximate a PD controller. Then, the discrete-time transfer function ($G(z)$) including the nominal plant and the approximate controller, is given by

$$G(z) = \frac{T_s^2 k_p z^2}{(1 + T_s^2 k_p + T_s k_d)z^2 - (T_s k_d + 2)z + 1}. \quad (40)$$

The Lyapunov stability and asymptotic stability of the system can both be compensated by setting the absolute value of the poles of the characteristic polynomial to <1. Note that the controller parameter of the PFC system is only T_{ref}, and the stability condition is satisfied by $T_{\mathrm{ref}} > 0$. Therefore, the PFC system utilized in this paper is a stable and optimal control system. Additionally, if the constraints on the PFC system are active, the stability is further improved because the plant motion is limited within the moveable range. Moreover, the robustness of the joint space controller is compensated by the accurate disturbance estimate of the IDOB. In the steady-state, the disturbance estimate is accurate for disturbances within the torque constraint. Additionally, the estimated excessive disturbance is canceled by the imposed torque constraints, which is not possible with conventional DOBs without the said constraints. This contributes to stable IDOB estimations for motion and disturbance, which is to say that the joint space controller configured by the IDOB and PFC systems is both stable and robust. The proposed method utilizes a joint space position control system that compensates for robustness and stability under the constraints as an inner-loop controller. Therefore, the robustness of the proposed method is compensated by utilizing the IDOB, which is similar to conventional DOB systems [32]. The implicit force control law is a simple feedback control system based on position control. The inverse kinematics conducted are numerically stable with a high-convergence performance [23]. Indeed, the proposed method is both robust and stable and produces accurate disturbance estimations.

IV. EXPERIMENTS

The experiments verify the performance of the proposed method for position/force control and demonstrate guaranteed motion against external forces. In the first experiment, the HPFC control performance by the proposed implicit force control was verified both with and without torque saturation. In the next experiment, the guaranteed motion against external forces without the force sensor of the proposed method was verified. In an additional experiment, the utilization of manipulator redundancy by the target closed-loop response time, which is a controller parameter on PFC, was verified. The three-link manipulator shown in Fig. 5 was utilized to verify the proposed method. The manipulator has three DC motors with encoders (harmonic-drive systems) in each joint. A load cell as a one-axis force sensor (A&D Corporation) was attached to the tip of the end-effector of the robot. The control system was implemented by a digital signal processor (sBOXII by MIS Corporation). The physical parameters comprised link distance ($\{l_1, l_2, l_3\} = 0.20$ m) and mass

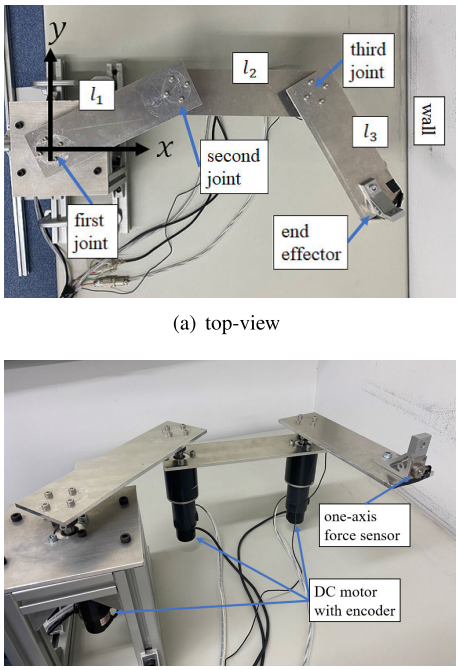

(a) top-view

(b) side-view

FIGURE 5. Experiment configuration.

($\{m_1, m_3, m_5\} = 0.22$ kg, $\{m_2, m_4\} = 0.77$ kg). The time constant of the lowpass filter for the force sensor was set to 0.05 s. All experimental systems were discretized by $T_s = 0.001$ s. The maximum outputs of each link torque were $\tau_{\mathrm{limit},q_1} = \tau_{\mathrm{limit},q_2} = 20.7360$ Nm for the first and second joints, respectively, and $\tau_{\mathrm{limit},q_3} = 12.6720$ Nm for the third joint. These values were determined from the specifications of the maximum continuous current of each motor driver. Additionally, a saturation function utilizing these values was programmed for the plant input as well as for the IDOB input in all control systems.

A. CONTROLLER SETUP

The experimental verification compared conventional HPFC utilizing DOB-based acceleration control and DOB-based resolved acceleration control (DRAC) [38] for the workspace position control utilizing the proposed reference generation with the proposed method. Through comparison with PHFC, it is evident that the proposed method considering torque saturation by the joint space position controller has equivalent control performance for position and force with respect to conventional methods. Moreover, through comparison with DRAC, the effectiveness of the position/force control by the joint space control with the torque constraints was verified. The IDOB for all controllers was tuned by the pole placement method with $[-40, -41, -42, -43, -44, -45, -46, -47, -48]$ and the nominal inertia matrix $\boldsymbol{J}_n = \mathrm{diag}(2.6683, 1.6772, 0.8155)$. The $\boldsymbol{J}_n$ parameter was obtained by modeling with the physical parameters. Additionally, the initial state estimates for the IDOB utilized the initial angle reference

(q_0^{ref}) for the initial state reference calculated in advance offline. If the initial state estimates are 0, the control system other than the proposed method will run out of control by singular point. This is because the initial state of the robot in the experiments was a singular point, and the Jacobian matrix was overestimated because of the singularity. By utilizing the initial angle reference as the initial observer state, the singular point of the Jacobian matrix was easily avoided. For all results, the position in the workspace was derived by utilizing the forward kinematics of the joint angle estimates by the IDOB.

The implicit controller gain was set as $K_f = 10F_x^{\mathrm{ref}}$ and was designed as an adaptive gain considering contact velocity. In the experiments IV-B and IV-C, the number of coincidence points for the target closed-loop response time of the PFC systems of each joint were $n = 3$ and $T_{\mathrm{ref},q_1} = T_{\mathrm{ref},q_2} = T_{\mathrm{ref},q_3} = 1.0$ s. The performance of the manipulator control of the proposed method was improved by utilizing redundancy with modified target closed-loop response times, the results of which were demonstrated in experiment IV-D. Moreover, the weight parameters of the inverse kinematic were set to $\{w_1, w_2, w_3\} = 10^2, 10^2, 10^1$.

The compared control systems can be represented by the equations for the control input, which, for HPFC, can be expressed as

$$\boldsymbol{\tau} = \boldsymbol{J}_n\{\boldsymbol{q}^{ref} + \boldsymbol{\tau}_{\mathrm{d}}\}, \tag{41}$$
$$= \boldsymbol{J}_n\{\boldsymbol{q}_{\mathrm{pos}}^{ref} + \boldsymbol{q}_{\mathrm{force}}^{\mathrm{ref}} + \boldsymbol{\tau}_{\mathrm{d}}\}, \tag{42}$$
$$\boldsymbol{q}_{\mathrm{pos}}^{ref} = \boldsymbol{K}_{phx}\boldsymbol{J}_{aco}^{+}\{\boldsymbol{S}(\boldsymbol{X}_0^{\mathrm{ref}} - \hat{\boldsymbol{X}}) - K_{dhx}\dot{\boldsymbol{q}} \tag{43}$$
$$\boldsymbol{q}_{\mathrm{force}}^{ref} = \boldsymbol{K}_{phf}\boldsymbol{J}_{aco}^{T}\{(\boldsymbol{I} - \boldsymbol{S})(\boldsymbol{F}^{\mathrm{ref}} - \boldsymbol{F}^{\mathrm{res}}), \tag{44}$$

and, for DRAC, as

$$\boldsymbol{\tau} = \boldsymbol{J}_n\{\boldsymbol{q}^{ref} + \boldsymbol{\tau}_{\mathrm{d}}\}, \tag{45}$$
$$= \boldsymbol{J}_n\boldsymbol{J}_{aco}^{+}\{\boldsymbol{K}_{px}(\boldsymbol{X}^{\mathrm{ref}} - \hat{\boldsymbol{X}}) - \boldsymbol{K}_{dx}\dot{\boldsymbol{q}} - \dot{\boldsymbol{J}}_{aco}\dot{\boldsymbol{q}}\}, \tag{46}$$

where ($\boldsymbol{K}_{phx}$, $\boldsymbol{K}_{px}$) and ($\boldsymbol{K}_{dhx}$, $\boldsymbol{K}_{dx}$) denote the proportional and differential gain matrices on the position control part, respectively, $\boldsymbol{K}_{phf}$ is a proportional gain matrix on the force control part, and $\boldsymbol{S}$ denotes the select matrix (diag(0,1,1)). $\boldsymbol{J}_{aco}^{+}$ denotes the pseudo-inverse matrix of $\boldsymbol{J}_{aco}$. A square matrix does not require the pseudo-inverse matrix, however, the pseudo-inverse matrix can treat singular points, so it is used in this paper. The position controller includes velocity feedback on the force control axis, which is introduced to suppress the impact force caused by the velocity. The IDOB and the reference generator in DRAC are the same as the proposed method. These parameters were adjusted by trial and error through each experiment.

B. HYBRID POSITION/FORCE CONTROL

The control performance of the proposed method when it comes into contact with a stationary rigid environment was verified. Because of input torque saturation, conventional force control methods can cause unstable behavior, such as hunting motion and runaway, when the system comes into contact with rigid objects. The proposed method considers unstable behavior by imposing the input constraints. In this experiment, two force references for the x-axis were considered: 2 and 5 N. In the steady state on the force tracking, the 2 N force reference did not cause torque saturation but the 5 N force reference did.

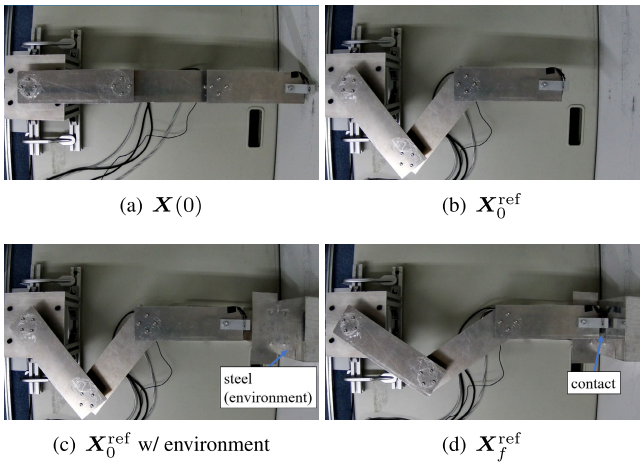

(a) $\boldsymbol{X}(0)$ (b) $\boldsymbol{X}_0^{\mathrm{ref}}$ (c) $\boldsymbol{X}_0^{\mathrm{ref}}$ w/ environment (d) $\boldsymbol{X}_f^{\mathrm{ref}}$

FIGURE 6. An example snapshot of experiment IV-B.

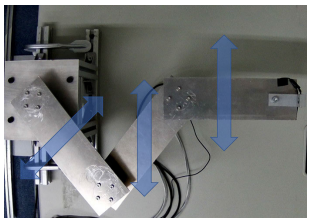

FIGURE 7. Experiments setup and configuration for IV-C. The blue arrows denote the external force direction with pull motion by the hand of the experimenter.

The verified control low began from the initial position $\boldsymbol{X}(0) = [x(0)\ y(0)\ \phi(0)] = [0.6\ \ 0\ \ 0]$ and then moved to the initial state of position/force control $\boldsymbol{X}_0^{\mathrm{ref}} = [x_0^{\mathrm{ref}}\ y_0^{\mathrm{ref}}\ \phi_0^{\mathrm{ref}}] = [0.45\ \ 0\ \ 0]$; the position and force were controlled from around 30 s. The reference for position and force control was $\boldsymbol{X}_f^{\mathrm{ref}} = [F_x^{\mathrm{ref}}\ \ y^{\mathrm{ref}}\ \ \phi^{\mathrm{ref}}] = [(2 \text{ or } 5 \text{ N})\ \ 0 \text{ m}\ \ 0 \text{ rad}]$. The F_x^{ref} was converted by the scheme described in III-B. Fig. 6 shows a snapshot of the experiments. In Fig. 6(b)-(c), a steel mount was installed as the environment, and the force was controlled by contact with the steel. The switching of references was performed manually. In the proposed method, the workspace position reference is based on (15). The attitude angle of the end effector was controlled. This is because the force sensor attached to the end-effector was uniaxial, and it is impossible to perform appropriate force control without proper attitude control. Additionally, since the position control of the workspace and the joint space is independent in the proposed method, the joint position control utilizing the angle reference ($\boldsymbol{q}_0^{\mathrm{ref}}$) calculated in advance offline was utilized to

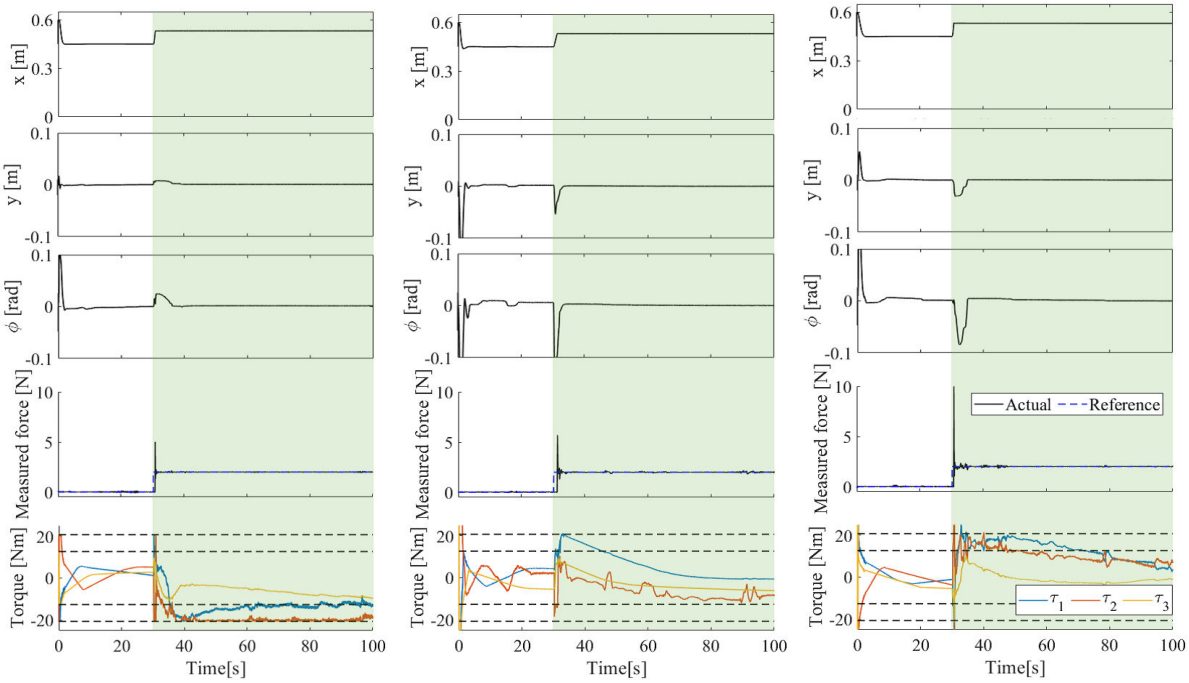

(a) prop. (b) conv. HPFC (c) conv. DRAC

FIGURE 8. Experimental result with $F_x^{\mathrm{ref}} = 2$N on IV-B. The filled area on the results denotes the position/force control period. In the torque results, the dashed line denotes the torque limitations ($\tau_{\mathrm{limit},q_1,q_2,q_3}$).

move from $\boldsymbol{X}(0)$ to $\boldsymbol{X}_0^{\mathrm{ref}}$. It is difficult to control the attitude between each link with a conventional workspace-based control system, but the proposed method can easily determine the initial posture (i.e., elbow up or elbow down). Note that it is possible to control the attitude by utilizing a suitable input in the null space, even in conventional control systems.

For HPFC, the gain matrices were set as (2N): $\boldsymbol{K}_{phx} = \{\mathrm{diag}(30, 30, 30)\}, \boldsymbol{K}_{dhx} = 2\sqrt{\boldsymbol{K}_{phx}}, \boldsymbol{K}_{phf} = \mathrm{diag}(40, 40, 40)$, and (5N): $\boldsymbol{K}_{phx} = \{\mathrm{diag}(30, 30, 30)\}, \boldsymbol{K}_{dhx} = 2\sqrt{\boldsymbol{K}_{phx}}, \boldsymbol{K}_{phf} = \mathrm{diag}(20, 20, 20)$. For DRAC, the gain matrices were set as (2N): $\boldsymbol{K}_{px} = \mathrm{diag}(15, 15, 15)$ and $\boldsymbol{K}_{dx} = 2\sqrt{\boldsymbol{K}_{px}}$, and (5N): $\boldsymbol{K}_{px} = \mathrm{diag}(30, 30, 30)$ and $\boldsymbol{K}_{dx} = 2\sqrt{\boldsymbol{K}_{px}}$.

The experimental results for $F_x^{\mathrm{ref}} = 2$ N with each controller are shown in Fig. 8, from which it is evident that, for the proposed method, the maximum reaction force (impact force) obtained from the force sensor with a lowpass filter is 5.0152 N, the time from force control start to contact is 522 ms, and the mean force tracking error for 50-100 s (steady state) is 0.0032 N. For HPFC, the maximum reaction force is 5.6958 N, the time from force control start to contact is 1,070 ms, and the mean tracking error for 50-100 s is 0.0008 N. For DRAC, the maximum force is 10.2835 N, the time from force control start to contact is 517 ms, and the mean force tracking error for 50-100 s is -0.0007N. From these results, it is evident that the proposed method has a comparable control performance with respect to position/force control as conventional methods. Furthermore, for the proposed method, the fluctuations are minimal for attitude and position; moreover, it has a smaller maximum reaction force than HPFC, and the contact time is shorter. The proposed method also has a smaller maximum reaction force than DRHC, but the contact time is equivalent. Indeed, the proposed method can treat impact force suppression and high-speed motion control at the same time; however, the tracking error of the force is slightly larger than conventional methods, and unexpected torque saturation occurs, both of which can be attributed to the target response time design. Accordingly, this error can be improved (or removed altogether) by modifying the tune-up, and IV-D shows its result. In light of this information, it is evident that the proposed method is useful for securing precise motion control, even if the torque is not saturated.

The experimental results for $F_x^{\mathrm{ref}} = 5$ N with each controller are shown in Fig. 9, from which it is evident that the torque of each controller is saturated in the steady state, which is to say that each controller realizes incomplete force control with respect to x-axis force control. For the proposed method, the maximum reaction force obtained from the force sensor with a lowpass filter is 8.9371 N, the time from force control start to contact is 520 ms, and the mean force tracking error for 50-100 s is 0.0010 N. For conventional HPFC, the maximum reaction force is 9.3942 N, the time from force control start to contact is 899 ms, and the mean force tracking error for 50-100 s is 0.0809 N. For conventional DRAC, the maximum reaction force is 15.2608 N, the time from force control start to contact is 434 ms, and the mean tracking error for 50-100 s is 0.1835 N. Overall, for force control, the proposed method can better reduce impact force while achieving high-speed motion compared with conventional

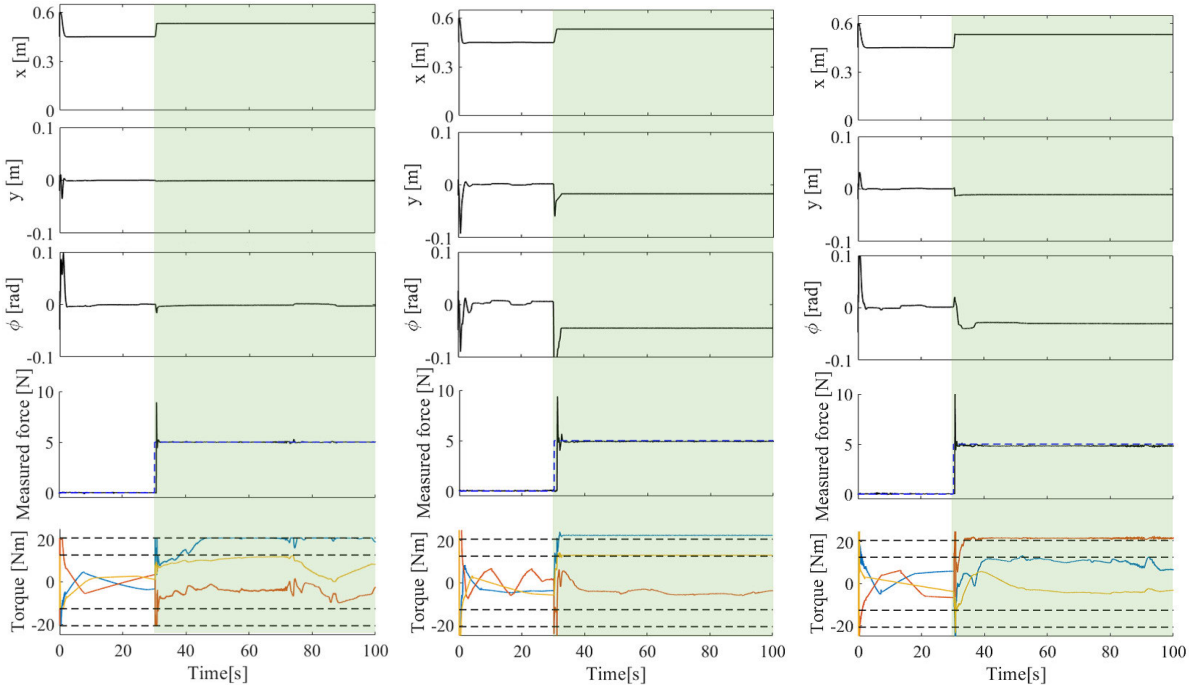

(a) prop. (b) conv. HPFC (c) conv. DRAC

FIGURE 9. Experimental result with $F_x^{\mathrm{ref}} = 5\mathrm{N}$ on IV-B. The filled area on the results denotes the position/force control period. In the torque results, the dashed line denotes the torque limitations ($\tau_{\mathrm{limit},q_1,q_2,q_3}$).

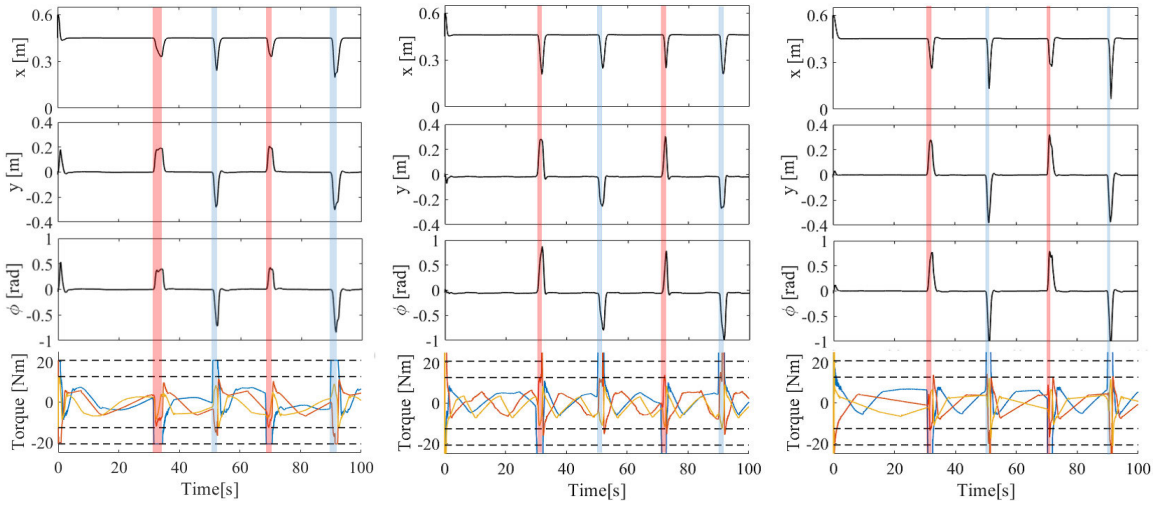

(a) prop. (b) HPFC (c) DRAC

FIGURE 10. Experimental results of l_1 on IV-C. In the filled area with red on the results, the first link was moved to the left side ($q < y$) by force with a hand. In the filled area with blue on the results, the first link was moved to the right side ($y < q$) by force with the hand.

HPFC, which makes a hunting motion (bouncing motion) at the time of contact. The results confirm that the DRAC system results in both a large impact force and tracking error. With respect to implicit workspace control, in using the DRAC system, it was difficult to control the force while considering attitude control. By contrast, the proposed method succeeds in suppressing the bouncing motion caused by contact with a rigid environment by considering the torque saturation and implicit control strategy. Furthermore, the time from force control start to contact for the proposed method are almost the same by the adaptive gain. Thus, the joint space-based implicit control strategy is useful for stable force control system implementations. With respect to the position control results, the results at y and ϕ show that the proposed

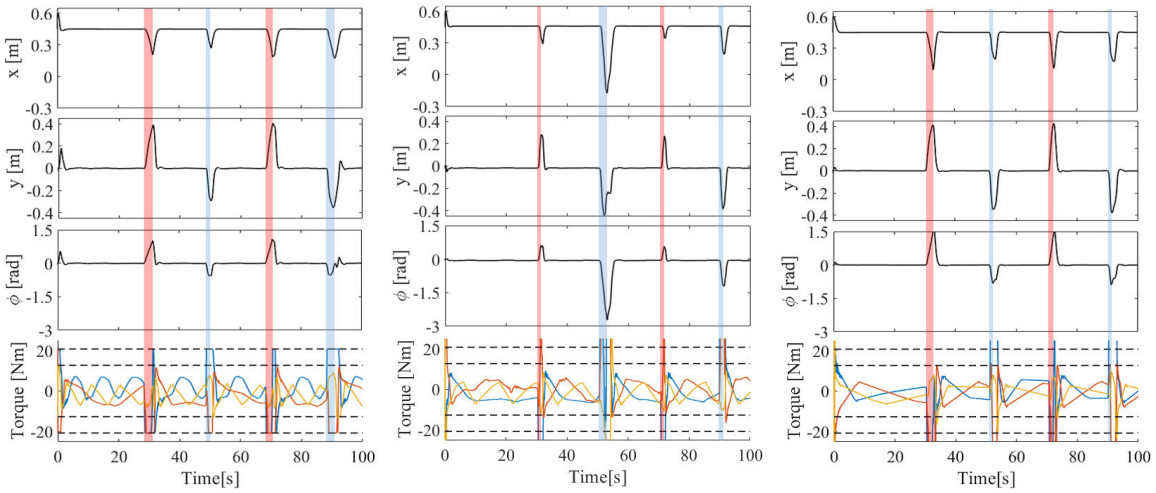

(a) prop. (b) HPFC (c) DRAC

FIGURE 11. Experimental results of l_2 on IV-C. In the filled area with red on the results, the first link was moved to the left side ($q < y$) by force with the hand. In the filled area with blue on the results, the first link was moved to the right side ($y < q$) by force with the hand.

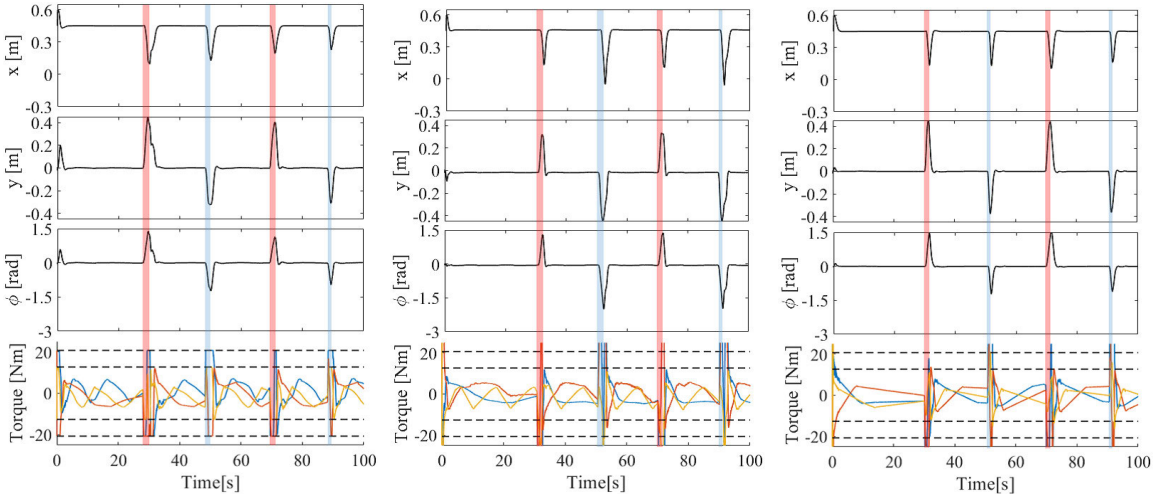

(a) prop. (b) HPFC (c) DRAC

FIGURE 12. Experimental results of l_3 on IV-C. In the filled area with red on the results, the first link was moved to the left side ($q < y$) by force with the hand. In the filled area with blue on the results, the first link was moved to the right side ($y < q$) by force with the hand.

method has a better tracking performance than the others. The torque variation with the initial position control period is generated by the disturbance estimates due to tracking errors with nonlinear friction. For the conventional methods, since the tracking errors are caused by torque saturation after contact, they cannot correct the position and attitude by the torque saturation after contact. Overall, the results suggest that, for conventional methods, the torque calculated from the controller is clearly saturated. Additionally, vibrational motion and a large error in the conventional method is caused. However, the torque violated the constraint is removed by the saturation function at the plant input and IDOB input, therefore, unstable motion is avoided. Because the robot utilizes the uniaxial force sensor, precision force control cannot be realized unless accurate attitude control is performed. By contrast, the results demonstrate that the proposed method performs well with respect to position/force control when considering the torque constraint via the acceleration reference. Moreover, the response time can be designed as a constant when considering the saturation of each actuator. In essence, the proposed method can avoid excessive control inputs and minimize the predicted tracking error via the optimization problem in the joint space. Consequently, the fluctuations in attitude and position are suppressed, and the proposed method is able to achieve appropriate control with a small number of sensors, whereas the conventional

methods result in undesired motion that should be avoided.

C. GUARANTEED MOTION AGAINST EXTERNAL FORCES

A control system considering torque saturation is useful for guaranteeing motion generation against external forces when making unexpected contact. The robot with the torque-bounded control system opposes the external force until the torque is saturated, but it moves according to the force that takes place after torque saturation. This behavior is essential for the collaborative works of people and robots, i.e., robots that make contact with people and robots that handle deformable objects. The proposed method has the potential to succeed in these areas. Fig. 7 shows a configuration for the experiment. In the experiment, after the initial position control, the experimenter forcibly applied an external force of roughly $\pi/2$ [rad] to each link (i.e., the experimenter pushed and pulled each link by hand). The controller parameters utilize the same as 5 N of experiment IV-B. Note that the initial values of the proposed method denote the joint space position reference, but, in this verification, the initial values were set as the workspace position references to evaluate the workspace behavior.

The experimental results of each link are shown in Figs. 10-12, from which it is evident that the proposed method can control the robot when considering torque saturation regardless of which part of the robot arm comes into contact. Moreover, the position and attitude increase monotonically after torque saturation. Therefore, the proposed method is successful in adapting to external forces while considering torque constraints. Additionally, it constantly generates motion that suppresses overshoot and vibration within an explicit torque range, and thus, it generates stable manipulator motion. By contrast, the HPFC system causes large and unwanted motion, especially in the result of l_2. In essence, the HPFC is dangerous because it creates excessive reactions due to excessive torque. The same can be said for the DRAC system. Excessive reactions are problematic because they can cause the joints to behave unexpectedly.

For the proposed method, it may be possible to realize more advanced and intelligent control to improve overall control performance if the reaction torque is utilized in the controller. Therefore, the proposed method is expected to integrate and extend with reaction torque observer [39]–[41], which utilizes an actuator as a force sensor for each joint.

D. MODIFICATION OF T_{ref}

This section aims to improve the tracking control performance for experiment IV-B for a force of 2 N and reduce the reaction for an impact force of 5 N. In other words, it is verified that the proposed method can independently adjust the control response of each link and easily utilize redundancy.

Fig. 13(a) shows the results of improving the tracking control performance in IV-B for a force of 2 N. The target

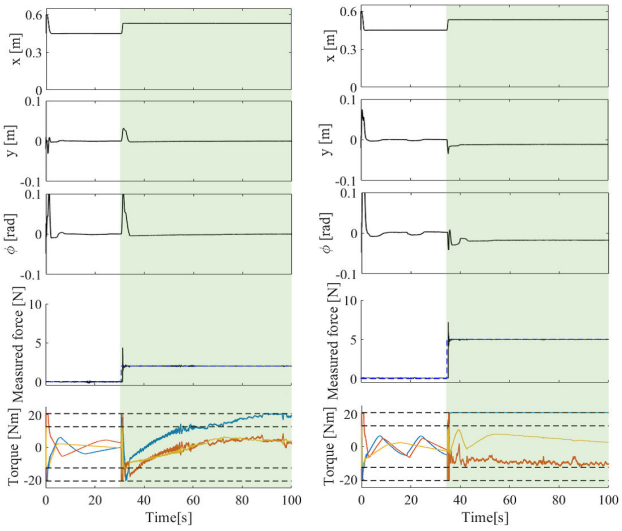

(a) Trackability improvement (b) Impact force improvement

FIGURE 13. Experimental results on IV-D.

settling times for the designed PFC system are $T_{\mathrm{ref},q_1} = 1.0$ s, $T_{\mathrm{ref},q_2} = 1.0$ s, and $T_{\mathrm{ref},q_3} = 0.7$ s. In the results of experiment IV-B, a tracking error can be observed in the steady-state force (0.0032N). Therefore, the target response time of q_3 should be decreased to effectively track the attitude angle and force. Moreover, the maximum reaction force is 4.3555 N, the time from force control start to contact is 544 ms, and the mean force tracking error for 50 $-$100 s is $-$0.0004 N. These results show an improved tracking error for the steady state. The proposed method can be widely and practically applied, since the response time of each actuator can be adjusted individually.

Fig. 13(b) shows the results of reducing the impact force. The target settling times for the designed PFC system are $T_{\mathrm{ref},q_1} = 1.2$ s, $T_{\mathrm{ref},q_2} = 0.5$ s, and $T_{\mathrm{ref},q_3} = 0.7$ s. The maximum reaction force is 7.1967 N, and the time from force control start to contact is 482 ms. Consequently, the impact force is suppressed, and high-speed control is successfully performed. Therefore, the control system can be adjusted more intuitively and easily than conventional methods. However, since the focus in this experiment concerns force control, tracking errors remain in attitude and position control after the saturation of the first joint torque. Therefore, a control system design that takes the force reference into account is required to achieve attitude and position control before contact is made.

V. CONCLUSION

In this paper, a robust HPFC strategy based on joint space position control considering torque saturation for an MDoFM was proposed. The proposed method is very useful compared with conventional control systems. The experimental results show that the control system considering torque saturation is effective in improving guaranteed motion generation against external forces and control performance. In future studies, an optimal adjustment method for the target response time

of each link based on control targets or handled tasks is desired. The proposed method can be easily implemented in high dimensional systems by utilizing the inverse kinematics as well as by decoupling each joint by DOB-based control. Additionally, it is particularly effective for human-robot systems and has a wide range of practical applications, such as bilateral control, driving force control, and conventional HPFC control systems.

REFERENCES

[1] M. H. Raibert and J. J. Craig, "Hybrid position/force control of manipulators," *J. Dyna. Syst., Meas., Control*, vol. 103, no. 2, pp. 123–133, 1981.

[2] T. Yoshikawa, "Dynamic hybrid position/force control of robot manipulators-description of hand constraints and calculation of joint driving force," *IEEE J. Robot. Autom.*, vol. 3, no. 5, pp. 386–392, Oct. 1987.

[3] S. Sakaino, T. Sato, and K. Ohnishi, "Precise position/force hybrid control with modal mass decoupling and bilateral communication between different structures," *IEEE Trans. Ind. Informat.*, vol. 7, no. 2, pp. 266–276, May 2011.

[4] Y. Hasegawa, T. Kitamura, S. Sakaino, and T. Tsuji, "Bilateral control of elbow and shoulder joints using functional electrical stimulation between humans and robots," *IEEE Access*, vol. 8, pp. 15792–15799, 2020.

[5] S. Xu, B. He, Y. Zhou, Z. Wang, and C. Zhang, "A hybrid position/force control method for a continuum robot with robotic and environmental compliance," *IEEE Access*, vol. 7, pp. 100467–100479, 2019.

[6] H. Cao, X. Chen, Y. He, and X. Zhao, "Dynamic adaptive hybrid impedance control for dynamic contact force tracking in uncertain environments," *IEEE Access*, vol. 7, pp. 83162–83174, 2019.

[7] Q. Xu, "Design and smooth position/force switching control of a miniature gripper for automated microhandling," *IEEE Trans. Ind. Informat.*, vol. 10, no. 2, pp. 1023–1032, May 2014.

[8] Z. Li, S. S. Ge, and S. Liu, "Contact-force distribution optimization and control for quadruped robots using both gradient and adaptive neural networks," *IEEE Trans. Neural Netw. Learn. Syst.*, vol. 25, no. 8, pp. 1460–1473, Aug. 2014.

[9] Q. Yang, C. Xie, R. Tang, H. Liu, and R. Song, "Hybrid active control with human intention detection of an upper-limb cable-driven rehabilitation robot," *IEEE Access*, vol. 7, pp. 83162–83174, 2019.

[10] H. Park, J. Park, D.-H. Lee, J.-H. Park, M.-H. Baeg, and J.-H. Bae, "Compliance-based robotic peg-in-hole assembly strategy without force feedback," *IEEE Trans. Ind. Electron.*, vol. 64, no. 8, pp. 6299–6309, Aug. 2017.

[11] A. Garcia, V. Girbes-Juan, J. E. Solanes, L. Gracia, C. Perez-Vidal, and J. Tornero, "Human-robot cooperation for surface repair combining automatic and manual modes," *IEEE Access*, vol. 8, pp. 154024–154035, 2020.

[12] N. Hogan, "Impedance control: An approach to manipulation: Part I—Theory," *J. Dyn. Syst., Meas., Control*, vol. 107, no. 2, pp. 1–7, 1985.

[13] R. Kikuuwe, "Torque-bounded admittance control realized by a set-valued algebraic feedback," *IEEE Trans. Robot.*, vol. 35, no. 5, pp. 1136–1149, Oct. 2019.

[14] Q. Xu and X. Sun, "Adaptive impedance control of robots with reference trajectory learning," *IEEE Access*, vol. 8, pp. 104967–104976, 2020.

[15] M. Bogdanovic, M. Khadiv, and L. Righetti, "Learning variable impedance control for contact sensitive tasks," *IEEE Robot. Autom. Lett.*, vol. 5, no. 4, pp. 6129–6136, Oct. 2020.

[16] R. Ikeura and H. Inooka, "Variable impedance control of a robot for cooperation with a human," in *Proc. IEEE Int. Conf. Robot. Autom.*, May 1995, pp. 3097–3102.

[17] L. Roveda, N. Castaman, P. Franceschi, S. Ghidoni, and N. Pedrocchi, "A control framework definition to overcome position/interaction dynamics uncertainties in force-controlled tasks," in *Proc. IEEE Int. Conf. Robot. Autom. (ICRA)*, May 2020, pp. 6819–6825.

[18] G. Ferretti, G. Magnani, and P. Rocco, "Toward the implementation of hybrid position/force control in industrial robots," *IEEE Trans. Robot. Automat.*, vol. 13, no. 6, pp. 838–845, Dec. 1997.

[19] J. Roy and L. L. Whitcomb, "Adaptive force control of position/velocity controlled robots: Theory and experiment," *IEEE Trans. Robot. Autom.*, vol. 18, no. 2, pp. 121–137, Apr. 2002.

[20] G. Duelen, H. Munch, D. Surdilovic, and J. Timm, "Automated force control schemes for robotic deburring: Development and experimental evaluation," in *Proc. Int. Conf. Ind. Electron., Control, Instrum., Autom.*, Nov. 1992, pp. 912–917.

[21] M. P. Polverini, D. Nicolis, A. M. Zanchettin, and P. Rocco, "Implicit robot force control based on set invariance," *IEEE Robot. Autom. Lett.*, vol. 2, no. 3, pp. 1288–1295, Jul. 2017.

[22] K. Ohishi, H. N. Wa, and S. Ohtaki, "Robust motion control with consideration algorithm of joint torque saturation for redundant manipulator," in *Proc. 26th Annu. Conf. IEEE Ind. Electron. Soc. IEEE Int. Conf. Ind. Electron., Control Instrum. 21st Century Technol. Ind. Opportunities (IECON)*, Oct. 2002, pp. 2255–2260.

[23] T. Sugihara, "Solvability-unconcerned inverse kinematics by the Levenberg–Marquardt method," *IEEE Trans. Robot.*, vol. 27, no. 5, pp. 984–991, Oct. 2011.

[24] J. Richalet and D. O'Donovan, *Predictive Functional Control Principles and Industrial Applications*. London, U.K.: Springer-Verlag, 2009.

[25] J. Richalet, S. Abu El Ata-Doss, C. Arber, H. B. Kuntze, A. Jacubasch, and W. Schill, "Predictive functional control–application to fast and accurate robots," *IFAC Proc. Volumes*, vol. 20, no. 5, pp. 251–258, Jul. 1987.

[26] H. Liu and S. Li, "Speed control for PMSM servo system using predictive functional control and extended state observer," *IEEE Trans. Ind. Electron.*, vol. 59, no. 2, pp. 1171–1183, Feb. 2012.

[27] T. Satoh, K. Kaneko, and N. Saito, "Performance improvement of predictive functional control: A disturbance observer approach," in *Proc. 37th Annu. Conf. IEEE Ind. Electron. Soc. (IECON)*, Nov. 2011, pp. 617–622.

[28] S. Katsura, K. Irie, and K. Ohishi, "Wideband force control by position-acceleration integrated disturbance observer," *IEEE Trans. Ind. Electron.*, vol. 55, no. 4, pp. 1699–1706, Apr. 2008.

[29] M. Nakao, K. Ohnishi, and K. Miyachi, "A robust decentralized joint control based on interference estimation," in *Proc. IEEE Int. Conf. Robot. Autom.*, Mar./Apr. 1987, pp. 326–331.

[30] S. Komada, N. Machii, and T. Hori, "Control of redundant manipulators considering order of disturbance observer," *IEEE Trans. Ind. Electron.*, vol. 47, no. 2, pp. 413–420, Apr. 2000.

[31] E. Sariyildiz, H. Sekiguchi, T. Nozaki, B. Ugurlu, and K. Ohnishi, "A stability analysis for the acceleration-based robust position control of robot manipulators via disturbance observer," *IEEE/ASME Trans. Mechatronics*, vol. 23, no. 5, pp. 2369–2378, Oct. 2018.

[32] E. Sariyildiz, R. Oboe, and K. Ohnishi, "Disturbance observer-based robust control and its applications: 35th anniversary overview," *IEEE Trans. Ind. Electron.*, vol. 67, no. 3, pp. 2042–2053, Mar. 2020.

[33] W. Chen, J. Yang, L. Guo, and S. Li, "Disturbance-observer-based control and related methods—An overview," *IEEE Trans. Ind. Electron.*, vol. 63, no. 2, pp. 1083–1095, Feb. 2016.

[34] T. Umeno, T. Kaneko, and Y. Hori, "Robust servosystem design with two degrees of freedom and its application to novel motion control of robot manipulators," *IEEE Trans. Ind. Electron.*, vol. 40, no. 5, pp. 473–485, 1993.

[35] A. Shimada and N. Hatakeyama, "Movement control of two-wheeled inverted pendulum robots considering robustness," in *Proc. SICE Annu. Conf.*, Aug. 2008, pp. 3361–3366.

[36] K. J. Astrom and L. Rundqwist, "Integrator windup and how to avoid it," in *Proc. Amer. Control Conf.*, Jun. 1989, pp. 1693–1698.

[37] G. A. Kiener, D. Lehmann, and K. H. Johansson, "Actuator saturation and anti-windup compensation in event-triggered control," *Discrete Event Dyn. Syst.*, vol. 24, no. 2, pp. 173–197, Jun. 2014.

[38] J. Luh, M. Walker, and R. Paul, "Resolved-acceleration control of mechanical manipulators," *IEEE Trans. Autom. Control*, vol. 25, no. 3, pp. 468–474, Jun. 1980.

[39] X. Liu, F. Zhao, S. S. Ge, Y. Wu, and X. Mei, "End-effector force estimation for flexible-joint robots with global friction approximation using neural networks," *IEEE Trans. Ind. Informat.*, vol. 15, no. 3, pp. 1730–1741, Mar. 2019.

[40] A. C. Smith, F. Mobasser, and K. Hashtrudi-Zaad, "Neural-network-based contact force observers for haptic applications," *IEEE Trans. Robot.*, vol. 22, no. 6, pp. 1163–1175, Dec. 2006.

[41] T. Murakami, F. Yu, and K. Ohnishi, "Torque sensorless control in multidegree-of-freedom manipulator," *IEEE Trans. Ind. Electron.*, vol. 40, no. 2, pp. 259–265, Apr. 1993.

TAKASHI OHHIRA received the B.E. and M.E. degrees in engineering and design from the Shibaura Institute of Technology, Tokyo, Japan, in 2016 and 2018, respectively. He is currently pursuing the Ph.D. degree with the Graduate School of Science and Technology, Keio University, Japan.

His research interests include robotics, optimal control, and motion control.

KEINOSUKE YOKOTA was born in Tokyo, Japan, in 1996. He received the B.E. degree in system design engineering from Keio University, Yokohama, Japan, in 2019, where he is currently pursuing the master's degree with the School of Integrated Design Engineering.

His research interest includes motion control of two-wheeled wheelchairs.

SHUICHI TATSUMI received the B.E. degree in system design engineering from Keio University, Yokohama, Japan, in 2019, where he is currently pursuing the master's degree with the School of Integrated Design Engineering.

His research interests include driving force control and motion control for Omni-directional robots.

TOSHIYUKI MURAKAMI (Senior Member, IEEE) received the B.E., M.E., and Ph.D. degrees in electrical engineering from Keio University, Yokohama, Japan, in 1988, 1990, and 1993, respectively.

In 1993, he joined the Department of Electrical Engineering, Keio University, where he is currently a Professor with the Department of System Design Engineering. From 1999 to 2000, he was a Visiting Researcher with the Institute for Power Electronics and Electrical Drives, Aachen University of Technology, Aachen, Germany. His research interests include robotics, intelligent vehicles, mobile robots, and motion control. In the education project, he was a coordinator of the European Master on Advanced Robotics (EMARO), Erasmus Program, from 2008 to 2018. Since 2019, he has been a responsible person of the Japan Europe Master on Advanced Robotics (JEMARO), Erasmus and MEXT Program with the Faculty of Science and Technology, Keio University.